



Cite this: *Phys. Chem. Chem. Phys.*,  
2015, 17, 9552

## Interaction of gas phase oxalic acid with ammonia and its atmospheric implications†

Xiu-Qiu Peng,<sup>ab</sup> Yi-Rong Liu,<sup>b</sup> Teng Huang,<sup>b</sup> Shuai Jiang<sup>b</sup> and Wei Huang<sup>\*ab</sup>

Oxalic acid is believed to play an important role in the formation and growth of atmospheric organic aerosols. However, as a common organic acid, the understanding of the larger clusters formed by gas phase oxalic acid with multiple ammonia molecules is incomplete. In this work, the structural characteristics and thermodynamics of oxalic acid clusters with up to six ammonia molecules have been investigated at the PW91PW91/6-311++G(3df,3pd) level of theory. We found that oxalic acid forms relatively stable clusters with ammonia molecules, and that ionization events play a key role. The analyses of the thermodynamics and atmospheric relevance indicate that the heterodimer (H<sub>2</sub>C<sub>2</sub>O<sub>4</sub>)(NH<sub>3</sub>) shows an obvious relative concentration in the atmosphere, and thus likely participates in new particle formation. However, with increasing number of ammonia molecules, the concentration of clusters decreases gradually. Additionally, clusters of oxalic acid with ammonia molecules are predicted to form favorably in low temperature conditions and show high Rayleigh scattering intensities.

Received 4th January 2015,  
Accepted 20th February 2015

DOI: 10.1039/c5cp00027k

www.rsc.org/pccp

### Introduction

Atmospheric aerosols are known to be involved in many important processes, including changing the Earth's climate by modifying cloud precipitation and properties,<sup>1,2</sup> influencing the Earth's radiation budget by absorbing and scattering solar radiation, affecting human health and, possibly, enhancing the mortality rate (*e.g.*, due to particles less than 2.5 μm).<sup>3–5</sup> New particle formation (NPF) produces the majority of atmospheric aerosols.<sup>6</sup> In the past, a great amount of theoretical and experimental work has focused on NPF events to investigate the properties and structures of molecular clusters,<sup>7–21</sup> and both methods have provided valuable perception of the potential chemical mechanisms of particle formation. The formation of new particles involves two stages:<sup>22–25</sup> an initial nucleation stage forming a critical nucleus (~1–3 nm in diameter) and a subsequent growth stage in which the size of the critical clusters increases rapidly.<sup>24,26</sup> The initial stage is critical and important, because its chemical makeup and populations would affect the NPF events along with the nucleation rate. So far, the chemical

compositions of the critical nuclei and the identity of the chemical species that participate in NPF still remain as uncertainties related to aerosol production.

Among these studies, the nucleation of organic matter with sulfuric acid, water and ammonia, the dominant nucleating species in the atmosphere, has received increasing amounts of attention. As is known, organic acids exist generally in nature and play an important role in ice nucleation,<sup>27–30</sup> cloud condensation,<sup>31</sup> and the production of fine particulate matter.<sup>32,33</sup> The pioneering laboratory experiments on nucleation of organic acids by Zhang *et al.* and the theoretical study of Yu *et al.* have clearly shown that organic acids enhance the nucleation and growth of nanoparticles involving sulfuric acid.<sup>34,35</sup> Previously, Nadykto and Yu indicated that both organic acids and ammonia may efficiently stabilize the binary H<sub>2</sub>SO<sub>4</sub>–H<sub>2</sub>O clusters and that the organic acids actively interact with ammonia.<sup>36</sup> As the most common dicarboxylic acid in the Earth's atmosphere,<sup>37–40</sup> oxalic acid has been observed with a significant concentration and is the dominant organic acid found in the PM<sub>2.5</sub> atmospheric aerosols.<sup>41,42</sup> Furthermore, the analysis of field measurements<sup>43</sup> revealed a strong correlation between the cloud condensation nuclei (CCN) and oxalate concentrations, which indicated that oxalate may play an important role in the CCN activation. Zhang *et al.* showed that dicarboxylic acids can contribute to the aerosol nucleation process by binding to sulfuric acid and ammonia.<sup>6</sup> The theoretical investigation of Yu *et al.* predicted that oxalic acid significantly enhances the stability of ionic clusters, catalyzing prenucleation clusters with positive charges.<sup>44</sup> Moreover, Tao *et al.*<sup>45</sup> reported that the formation of neutral cores is the most

<sup>a</sup> School of Environmental Science & Optoelectronic Technology, University of Science and Technology of China, Hefei, Anhui 230026, China. E-mail: huangwei6@ustc.edu.cn

<sup>b</sup> Laboratory of Atmospheric Physico-Chemistry, Anhui Institute of Optics & Fine Mechanics, Chinese Academy of Sciences, Hefei, Anhui 230031, China

† Electronic supplementary information (ESI) available: The coordinates, harmonic frequencies (in cm<sup>-1</sup>) and IR intensities for (H<sub>2</sub>C<sub>2</sub>O<sub>4</sub>)(NH<sub>3</sub>)<sub>n</sub> (n = 1–6) isomers optimized at the PW91PW91/6-311++G(3df,3pd) level of theory, and the data for isomers with ammonia binding to either carboxyl and with relative single point energy above 6 kcal mol<sup>-1</sup>. See DOI: 10.1039/c5cp00027k

important step in the initial formation of oxalic acid and water clusters; recently, they predicted that thermodynamically stable  $\text{H}_2\text{C}_2\text{O}_4\text{-NH}_3$  core clusters may likely participate in NPF chemistry, and that their subsequent hydration is favorable compared to the monohydrates of oxalic acid.<sup>46</sup> The significance of the  $\text{H}_2\text{C}_2\text{O}_4\text{-NH}_3$  core to the subsequent hydration in the atmosphere is clear, however, what possible features could the clusters of oxalic acid with ammonia show at larger sizes? If the clusters of oxalic acid with ammonia at larger sizes demonstrate stable structures and a concentration similar to that of the  $\text{H}_2\text{C}_2\text{O}_4\text{-NH}_3$  core, these clusters may exist in the atmosphere and participate in the subsequent hydration. Thus, it is of interest and necessary to study the clusters of oxalic acid with more ammonia molecules. In this work, we investigate the initial ionization events of  $(\text{H}_2\text{C}_2\text{O}_4)(\text{NH}_3)_n$  ( $n = 1\text{--}6$ ), its atmospheric relevance, temperature dependence and Rayleigh light scattering properties at the molecular level. The structures and energies of the clusters  $(\text{H}_2\text{C}_2\text{O}_4)(\text{NH}_3)_n$  ( $n = 1\text{--}6$ ) are predicted using the basin-hopping (BH) method<sup>47–49</sup> coupled with density functional theory (DFT) calculations. To the best of our knowledge, there is no similar research on the ability of the BH global searching method to search for the low-lying isomers of  $(\text{H}_2\text{C}_2\text{O}_4)(\text{NH}_3)_n$  clusters. The BH approach was tested to be highly efficient for many atomic clusters, such as gold clusters,<sup>50–53</sup> boron clusters<sup>54</sup> and doped gold clusters.<sup>55</sup> A new sampling skill called compressed sampling was effectively introduced to BH coupled with DFT and verified by water, nitrate–water, oxalate–water clusters and chlorine–water clusters.<sup>56–58</sup>

## Theoretical methods

The initial geometries of the monomers and  $(\text{H}_2\text{C}_2\text{O}_4)(\text{NH}_3)_n$  ( $n = 1\text{--}6$ ) clusters in this study were searched using the BH method coupled with DFT. Generalized gradient approximation in the Perdew–Burke–Ernzerhof (PBE) functional and the double numerical plus d-functions (DND) basis set, implemented in DMol<sup>3</sup>,<sup>59</sup> were chosen for the structure optimization of this system. This method has been used to explore atomic and molecular systems in our previous studies.<sup>49,53–55,57,58,60–62</sup>

For each cluster, three separate BH searches, consisting of 1000 sampling steps at 3000 K starting with randomly generated molecular configurations, were performed.

The geometries were first optimized at the PW91PW91/6-31+G\* level of theory. The isomers located within 6 kcal mol<sup>-1</sup> of the global minimum were then selected and reoptimized by the PW91PW91/6-311++G(3df,3pd) level of theory implemented in the Gaussian 09 software package.<sup>63</sup> The PW91PW91 method has shown fine performance on clusters containing common organic acids, and its predictions<sup>36,44</sup> agree best with experiments compared to other density functionals. In order to make sure the results are consistent, another four methods ( $\omega\text{B97x-D}$ , M06-2X, CAM-B3LYP and B3LYP) were performed for the smallest clusters, including  $\text{NH}_3$ ,  $\text{C}_2\text{O}_2\text{H}_4$ ,  $(\text{C}_2\text{O}_2\text{H}_4)(\text{NH}_3)$  and  $(\text{C}_2\text{O}_2\text{H}_4)(\text{NH}_3)_2$ . We choose to use density functional instead of wave function theory methods (*i.e.* MP2) to compare with each

**Table 1** Calculated Gibbs free energy and free energy changes of  $\text{NH}_3$ ,  $\text{C}_2\text{O}_2\text{H}_4$ ,  $(\text{C}_2\text{O}_2\text{H}_4)(\text{NH}_3)$  and  $(\text{C}_2\text{O}_2\text{H}_4)(\text{NH}_3)_2$  using different DFT functionals with the 6-311++G(3df,3pd) basis set

Isomer	Functional	G (Hartree)	$\Delta G$ (kcal mol <sup>-1</sup> )
$\text{NH}_3$	$\omega\text{B97x-D}$	-56.550	
	M06-2X	-56.536	
	CAM-B3LYP	-56.541	
	B3LYP	-56.572	
	PW91PW91	-56.544	
$\text{C}_2\text{O}_2\text{H}_4$	$\omega\text{B97x-D}$	-378.337	
	M06-2X	-378.321	
	CAM-B3LYP	-378.333	
	B3LYP	-378.462	
	PW91PW91	-378.363	
$(\text{C}_2\text{O}_2\text{H}_4)(\text{NH}_3)$	$\omega\text{B97x-D}$	-434.891	-2.422
	M06-2X	-434.862	-3.324
	CAM-B3LYP	-434.891	-10.309
	B3LYP	-435.037	-1.420
	PW91PW91	-434.914	-4.172
$(\text{C}_2\text{O}_2\text{H}_4)(\text{NH}_3)_2$	$\omega\text{B97x-D}$	-491.435	0.988
	M06-2X	-491.393	-0.660
	CAM-B3LYP	-491.413	1.517
	B3LYP	-491.602	3.165
	PW91PW91	-491.455	-2.300

other like the work by Elm *et al.*<sup>20</sup> The computational costs could be largely reduced due to the absence of wave function theory, and the accuracy of the benchmark could be maintained because recent benchmark articles<sup>19,20</sup> provide the pool of potential density functional methods including those methods mentioned in this benchmark work. From the current benchmark work displayed in Table 1, the Gibbs free energy calculated by PW91 was closer to that calculated by M06-2X and  $\omega\text{B97x-D}$ , rather than CAM-B3LYP and B3LYP. In the cluster  $(\text{C}_2\text{O}_2\text{H}_4)(\text{NH}_3)$ , the free energy change calculated by PW91PW91 was very close to that calculated by M06-2X: the results were  $-4.172$  kcal mol<sup>-1</sup> and  $-3.324$  kcal mol<sup>-1</sup>, respectively. The differences between the free energy change calculated by PW91PW91 and the free energy change calculated by  $\omega\text{B97x-D}$  was 1.75 kcal mol<sup>-1</sup>. In the cluster  $(\text{C}_2\text{O}_2\text{H}_4)(\text{NH}_3)_2$ , the differences between the free energy change calculated by PW91PW91 and with other methods increased, but were near 3 kcal mol<sup>-1</sup>; this could be acceptable as the differences among the results of different functionals are supposed to increase with the increasing size of clusters.

For each stationary point, frequency calculations confirmed that no imaginary frequencies existed (details can be seen in the ESI<sup>†</sup>). The single-point energies of the selected isomers of the  $(\text{H}_2\text{C}_2\text{O}_4)(\text{NH}_3)_n$  ( $n = 1\text{--}6$ ) system were ultimately calculated at the DF-MP2-F12/vdz-f12 level of theory using Molpro 2010.1;<sup>64,65</sup> this level of theory has been proven to be accurate for single-point energy calculations for the  $(\text{C}_2\text{O}_2\text{H}_4)(\text{H}_2\text{SO}_4)_2$  ( $\text{H}_2\text{O}$ )<sub>*n*</sub> ( $n = 1\text{--}3$ ) and  $(\text{C}_2\text{O}_2\text{H}_4)(\text{HSO}_4^-)(\text{H}_2\text{SO}_4)(\text{H}_2\text{O})_n$  ( $n = 1\text{--}3$ ) systems.<sup>62</sup> The relative energies ( $\Delta E_{\text{rel}}$ ) were defined as the relative electronic energy of the global minimum. The ZPE-corrected binding energies ( $\Delta E_0$ ) and the relative energies ( $\Delta E_{\text{rel}}$ ) were obtained at a standard state of 0 K and 1 atm. The intermolecular enthalpies ( $\Delta H$ ) and Gibbs free energies

( $\Delta G$ ) were calculated at a temperature of 298.15 K and 1 atm. Subsequently, to better clarify the nature of the intramolecular hydrogen bond interactions of clusters of various sizes, the characteristics of the bond critical points (BCPs) were analyzed using the atoms in molecules (AIM)<sup>66</sup> approach by means of the Multiwfn program.<sup>67</sup> To study the non-covalent interaction (NCI) of oxalic acid with ammonia, the reduced density gradient (RDG) associated with the hydrogen binding regions in real space has been calculated using the Multiwfn program and visualized with the VMD program.<sup>68</sup> The RDG method presented by Yang and coworkers<sup>69</sup> has been validated to be convenient and effective for identifying non-covalent interactions.

To evaluate the Rayleigh scattering intensities and polarization ratios of oxalic acid with ammonia, the most common dicarboxylic acid and the dominant base in the atmosphere, the binding mean isotropic and anisotropic polarizabilities of all clusters were calculated at the CAM-B3LYP/aug-cc-pVDZ level of theory. The benchmark work for the smallest cluster subunits H<sub>2</sub>SO<sub>4</sub>, NH<sub>3</sub> and H<sub>2</sub>O was performed by Elm *et al.*<sup>70</sup> On the basis of this analysis, they found that CAM-B3LYP/aug-cc-pVDZ was a good compromise between efficiency and accuracy, yielding good agreement with both experimental and CCSD(T) values of the polarizability. Furthermore, the CAM-B3LYP functional has been successfully used in the calculation of various response properties such as polarizabilities,<sup>71,72</sup> absorption properties,<sup>73</sup> van der Waals  $C_6$ -coefficients,<sup>71</sup> and magnetic circular dichroism.<sup>74,75</sup> Additionally, CAM-B3LYP showed an adequate performance in calculating the hyper-Rayleigh scattering of large chromophores.<sup>76</sup> In this article, to find a suitable methodology for calculating the optical properties of the prenucleation clusters, a DFT functional with the aug-cc-pVDZ basis set analysis was performed for the smallest clusters including NH<sub>3</sub>, C<sub>2</sub>O<sub>2</sub>H<sub>4</sub>, (C<sub>2</sub>O<sub>2</sub>H<sub>4</sub>)(NH<sub>3</sub>) and (C<sub>2</sub>O<sub>2</sub>H<sub>4</sub>)(NH<sub>3</sub>)<sub>2</sub>. Its performance in calculating the mean isotropic polarizability was tested using  $\omega$ B97x-D, M06-2X, MP2, CAM-B3LYP and PW91 with the aug-cc-pVDZ basis set. The results are shown in Table 2; based on analysis of the results, CAM-B3LYP/aug-cc-pVDZ was found to be a good compromise between accuracy and efficiency, yielding good agreement with the MP2 values of the polarizability.

The light scattering intensities and the isotropic mean polarizabilities  $\bar{\alpha}$ , as well as the anisotropic polarizabilities  $\Delta\alpha$  and the relevant computational methods, have been given in our previous study.<sup>58</sup>

**Table 2** Calculated isotropic mean polarizabilities ( $\bar{\alpha}$ ) of NH<sub>3</sub>, C<sub>2</sub>O<sub>2</sub>H<sub>4</sub>, (C<sub>2</sub>O<sub>2</sub>H<sub>4</sub>)(NH<sub>3</sub>) and (C<sub>2</sub>O<sub>2</sub>H<sub>4</sub>)(NH<sub>3</sub>)<sub>2</sub> using different DFT functionals with the aug-cc-pVDZ basis set

Functional	NH <sub>3</sub>	C <sub>2</sub> O <sub>2</sub> H <sub>4</sub>	(C <sub>2</sub> O <sub>2</sub> H <sub>4</sub> )(NH <sub>3</sub> )	(C <sub>2</sub> O <sub>2</sub> H <sub>4</sub> )(NH <sub>3</sub> ) <sub>2</sub>
$\omega$ B97x-D	13.980	38.651	53.682	68.472
M06-2X	13.645	37.675	52.551	67.032
CAM-B3LYP	14.000	38.663	53.814	68.935
MP2	14.041	39.984	55.492	70.855
PW91PW91	14.993	41.795	58.532	75.362

## Results and discussion

### 3.1 Structures and energies

The geometry of the oxalic acid monomer in this work is a planar *trans* conformation ( $C_{2h}$  point group), with weak intramolecular hydrogen bonds to the carboxyl oxygen at neighboring carboxyl groups.<sup>6,44</sup> The representations of the (H<sub>2</sub>C<sub>2</sub>O<sub>4</sub>)(NH<sub>3</sub>)<sub>*n*</sub> (*n* = 1–6) conformations are defined using *m*–*n* notation. In this notation, “*m*” (*m* = I, II, III, IV, V and VI) denotes the number of ammonia molecules. “*n*” (*n* = a–d) is used to distinguish different isomers with the same value of *m*, ordered by increasing relative single point energy  $\Delta E_{\text{rel}}$ . The ZPE-corrected binding energies ( $\Delta E_0$ ) of the cluster were calculated using the following equation. The interaction enthalpies ( $\Delta H$ ) and free energy changes ( $\Delta G$ ) were calculated in the same way:

$$\Delta E_n = E_n - n \times E_{\text{NH}_3} - E_{\text{C}_2\text{O}_4\text{H}_2} \quad (1)$$

where *n* indicates the number of ammonia molecules in the cluster and  $E_n$  is the total energy;  $E_{\text{NH}_3}$  and  $E_{\text{C}_2\text{O}_4\text{H}_2}$  are the total energies for ammonia and oxalic acid. The binding energies of all isomers are shown in Table 3. The most stable structure of the H<sub>2</sub>C<sub>2</sub>O<sub>4</sub>–NH<sub>3</sub> isomers was consistent with the available reported structure.<sup>45,46</sup>

Fig. 1 displays the optimized structures of the global and local minima at the PW91PW91/6-311++G(3df,3pd) level of theory for (H<sub>2</sub>C<sub>2</sub>O<sub>4</sub>)(NH<sub>3</sub>)<sub>*n*</sub>. The lowest-energy structures of the (H<sub>2</sub>C<sub>2</sub>O<sub>4</sub>)(NH<sub>3</sub>)<sub>*n*</sub> (*n* = 1–6) clusters are ordered by the state of association (I, II, III, IV, V and VI). Isomers with ammonia binding to either carboxyl and with a relative single point energy above 6 kcal mol<sup>−1</sup> are displayed in Fig. S1 (ESI<sup>†</sup>), and the corresponding binding energies are shown in Table S1 (details can be seen in the ESI<sup>†</sup>). The intramolecular and intermolecular interaction distances and the corresponding isosurfaces are given in Fig. 2. For the H<sub>2</sub>C<sub>2</sub>O<sub>4</sub>–NH<sub>3</sub> complexes, the global minimum of the H<sub>2</sub>C<sub>2</sub>O<sub>4</sub>–NH<sub>3</sub> cluster is I-a. As shown in Fig. 2, two intermolecular hydrogen bonds are formed in cluster I-a: a stronger H···N bond with a length of 1.536 Å and a weaker O···H bond with a length of 2.154 Å. For the (H<sub>2</sub>C<sub>2</sub>O<sub>4</sub>)(NH<sub>3</sub>)<sub>2</sub> clusters, the global minimum is II-a. It is observed that the length of the stronger intermolecular H···N bond reduces to 1.211 Å from 1.536 Å, and the length of the adjacent covalent O–H bond increases from 1.067 Å to 1.304 Å. The global minimum of the (H<sub>2</sub>C<sub>2</sub>O<sub>4</sub>)(NH<sub>3</sub>)<sub>3</sub> clusters is III-a, with an enthalpy change  $\Delta H = -36.219$  kcal mol<sup>−1</sup>, and a free energy change  $\Delta G = -6.018$  kcal mol<sup>−1</sup>. The addition of the second ammonia produces a free energy change 2.743 kcal mol<sup>−1</sup> higher than that of (H<sub>2</sub>C<sub>2</sub>O<sub>4</sub>)(NH<sub>3</sub>); however, the addition of the third ammonia produces a free energy change  $-3.614$  kcal mol<sup>−1</sup> lower compared to that of (H<sub>2</sub>C<sub>2</sub>O<sub>4</sub>)(NH<sub>3</sub>)<sub>2</sub>. In this configuration, a proton from the donor H<sub>2</sub>C<sub>2</sub>O<sub>4</sub> transfers to the acceptor ammonia, and the length of the strong intermolecular H···N bond reduces to 1.097 Å, nearly to the nitrogen–hydrogen bond distances of ammonia. The length of the adjacent covalent O–H bond increases from 1.304 Å to 1.538 Å, forming an HC<sub>2</sub>O<sub>4</sub><sup>−</sup>/NH<sub>4</sub><sup>+</sup> ion pair. For the clusters of (H<sub>2</sub>C<sub>2</sub>O<sub>4</sub>)(NH<sub>3</sub>)<sub>*n*</sub> (*n* = 4–6), the distance of the intermolecular H···N bonds decreases as the

**Table 3** The relative single point energies  $\Delta E_{\text{rel}}$ , the ZPE-corrected binding energies ( $\Delta E_0$ ), intermolecular enthalpies ( $\Delta H$ ), free energy changes ( $\Delta G$ ) and Boltzmann averaged Gibbs free energies of  $(\text{H}_2\text{C}_2\text{O}_4)(\text{NH}_3)_n$  ( $n = 1-6$ ) (in kcal mol<sup>-1</sup>) based on PW91PW91/6-311++G(3df,3pd) calculations

<i>n</i>	Isomer	$\Delta E_{\text{rel}}$	$\Delta E_0$	$\Delta H$	$\Delta G$	Boltzmann averaged Gibbs free energy
1	I-a	0	-14.094	-14.612	-5.147	-5.147
2	II-a	0	-20.539	-21.630	-2.404	-0.797
	II-b	4.807	-15.732	-15.984	0.821	
3	III-a	0	-34.158	-36.219	-6.018	-4.447
	III-b	0.191	-33.966	-35.783	-5.689	
	III-c	0.430	-33.728	-35.755	-6.297	
	III-d	0.820	-33.338	-35.439	-5.671	
	III-e	5.670	-28.459	-29.893	-1.405	
	III-f	6.032	-28.126	-29.269	1.558	
4	IV-a	0	-37.308	-38.756	-1.449	5.284
	IV-b	0.747	-36.561	-38.001	-0.911	
	IV-c	0.895	-36.413	-38.333	-0.264	
	IV-d	2.710	-34.599	-36.395	1.594	
	IV-e	3.425	-33.883	-35.482	1.931	
	IV-f	3.834	-33.474	-35.271	3.018	
	IV-g	4.415	-32.893	-34.804	3.628	
	IV-h	5.190	-32.119	-33.991	3.405	
5	V-a	0	-44.356	-46.262	0.522	2.927
	V-b	0.708	-43.649	-45.712	1.749	
	V-c	1.040	-43.316	-45.413	1.595	
	V-d	1.232	-43.125	-44.954	1.501	
	V-e	1.895	-42.461	-44.601	2.377	
	V-f	2.209	-42.147	-44.560	4.416	
	V-g	2.531	-41.825	-44.488	5.360	
	V-h	3.772	-40.584	-42.668	3.470	
	V-i	4.031	-40.326	-42.694	5.744	
6	VI-a	0	-51.544	-54.332	3.495	12.667
	VI-b	1.808	-49.736	-52.098	4.483	
	VI-c	3.540	-48.004	-50.898	8.164	
	VI-d	4.697	-46.847	-49.662	8.886	
	VI-e	5.569	-45.975	-48.680	8.984	
	VI-f	5.975	-45.568	-48.295	9.129	

clusters grow to larger size. In the clusters  $(\text{H}_2\text{C}_2\text{O}_4)(\text{NH}_3)_4$ , some of the free energy changes are negative, and some are positive. For the clusters  $(\text{H}_2\text{C}_2\text{O}_4)(\text{NH}_3)_n$  ( $n = 5-6$ ), the free energy changes are all positive. This indicates that ionization events exist in the formation of  $(\text{H}_2\text{C}_2\text{O}_4)(\text{NH}_3)_n$  clusters and play a role in the stability of the oxalic acid and ammonia system; furthermore, three ammonia molecules are needed for oxalic acid dissociation.

### 3.2. Electron density and non-covalent interactions (NCI) analysis

Topological analysis of the electron density can prove the existence of the hydrogen bond in all clusters. So AIM theory<sup>66</sup> was applied here to deepen the understanding of the nature of the intermolecular hydrogen bond in the oxalic acid and ammonia system. To analyze the topological characteristics at the bond critical point, we used the electron density ( $\rho$ ), its Laplacian ( $\nabla^2\rho$ ), and the electronic energy density ( $E$ ), which is composed of the electronic kinetic energy density ( $G$ ) and the electronic potential energy density ( $V$ ),  $\rho$ , which is a good

estimate of the strength of the hydrogen bond.<sup>66</sup> The larger the  $\rho$  value, the stronger the hydrogen bond is. The values of the AIM topological parameters calculated using the Multiwfn program<sup>67</sup> for the hydrogen bonds between  $\text{H}_2\text{C}_2\text{O}_4$  and  $\text{NH}_3$  for all global minima are listed in Table 4. They indicate that hydrogen-bonded intermolecular interactions exist in these complexes, and that some intermolecular hydrogen bonds are relatively strong. The values of  $\nabla^2\rho$  and  $E$  indicate the nature of the interaction. A negative value of  $\nabla^2\rho$  indicates that there is a shared interaction, such as in a covalent bond, whereas a positive value of  $\nabla^2\rho$  indicates closed-shell system interactions, that is, ionic interactions, van der Waals forces, or hydrogen bonding.<sup>66</sup> On the other hand, if  $\nabla^2\rho$  is positive but  $E$  is negative, then the interaction is partly covalent in nature.<sup>77</sup> Here  $-G/V$  is chosen, as the balance between the positive value of  $G$  and the negative value of  $V$  may indicate the regions corresponding to covalent or non-covalent interactions. If  $-G/V$  is greater than 1, then the interaction is non-covalent. If the ratio is between 0.5 and 1, the interaction is partly covalent in nature, and when this ratio is less than 0.5, the interaction is a shared covalent interaction.<sup>78</sup> The structures of the global minima with their hydrogen bond distances and corresponding isosurfaces are shown in Fig. 2. As shown in Fig. 2 and Table 4, the length of the stronger intermolecular  $\text{H}\cdots\text{N}$  bond of the  $(\text{H}_2\text{C}_2\text{O}_4)(\text{NH}_3)_n$  ( $n = 1-6$ ) clusters is reduced from 1.536 Å to 1.055 Å. The relevant value of  $\rho$  increases from 0.0853 a.u. to 0.3338 a.u. The interaction of this  $\text{H}\cdots\text{N}$  bond is partly covalent in the dimer, with  $-G/V = 0.52$ , then tending toward shared covalent in the trimer. The coterminous  $\text{O}\cdots\text{H}$  bond increases from 1.067 Å to 1.735 Å. The relevant value of  $\rho$  reduces from 0.2671 a.u. to 0.0446 a.u. The interaction of this  $\text{O}\cdots\text{H}$  bond with  $-G/V = 0.44$  is covalent in the dimer, then becomes closer to partly covalent for the trimer, and becomes a hydrogen bond in the tetramer. From these values, the tetramer can be seen as the turning point of the proton transfer, verifying the former structures analysis. The  $-G/V$  values of the other hydrogen bonds formed between oxalic acid and ammonia are greater than 1, and these interactions are non-covalent. The relevant values of  $\rho$  range from 0.0106 a.u. to 0.0225 a.u., which fall within the generally accepted range of a hydrogen bond, which is the range from 0.002 to 0.035 a.u., and their corresponding Laplacians ( $\nabla^2\rho$ ) all fall within the proposed range from 0.024 to 0.139 a.u. of a hydrogen bond,<sup>79</sup> showing that there are hydrogen-bonded intermolecular interactions in the oxalic acid and ammonia system.

The non-covalent interaction (NCI) index based on the correlation between the reduced density gradient and the electron density has been presented by Yang and coworkers.<sup>69,80</sup> The reduced density gradient

$$s = \frac{1}{2(3\pi^2)^{1/3}} \frac{|\nabla\rho|}{\rho^{4/3}} \quad (2)$$

is a fundamental dimensionless quantity in DFT, which is used to describe the deviation from a homogeneous electron distribution.<sup>69,81</sup> To some extent, the NCI analysis method can be seen as

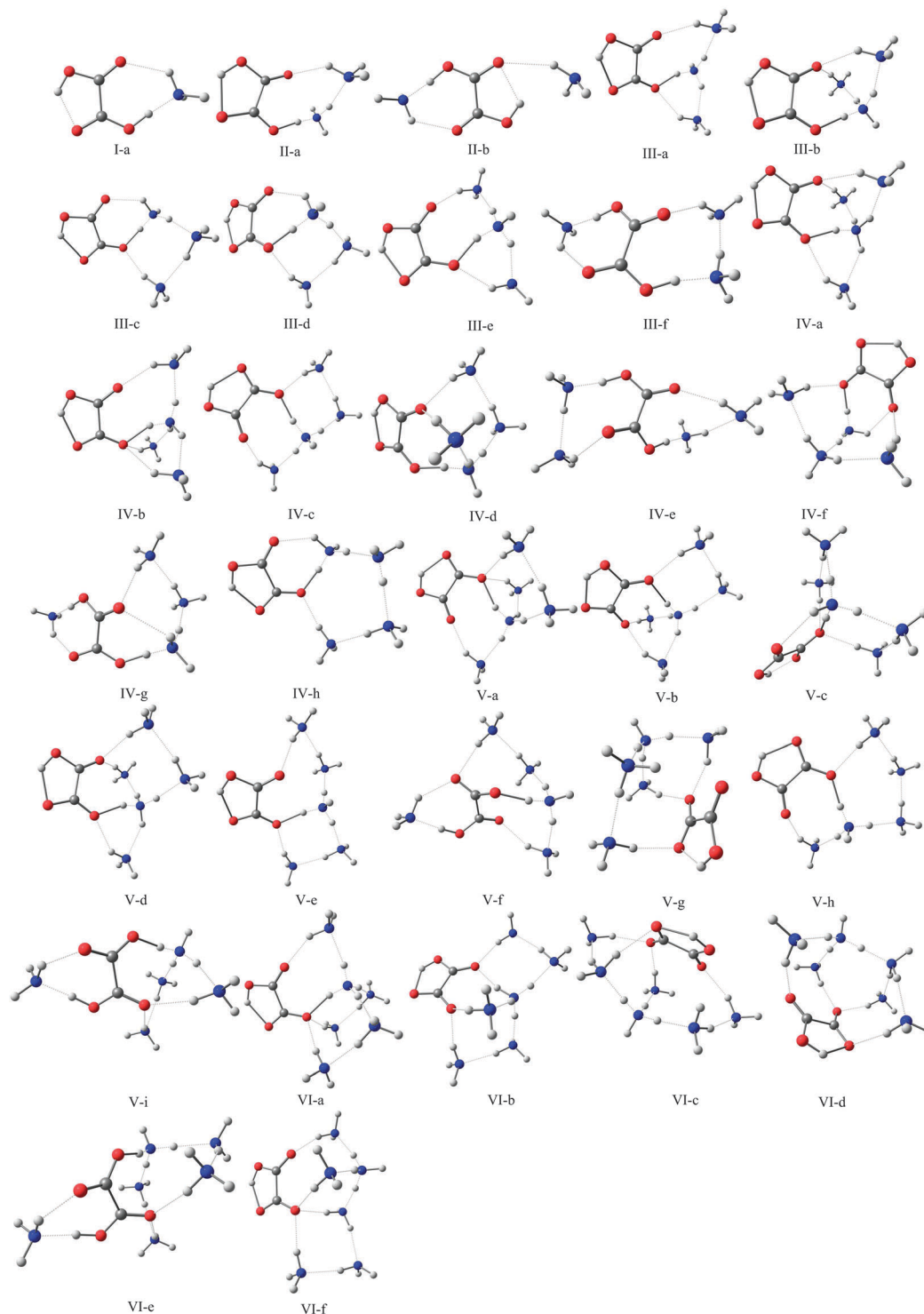


Fig. 1 The optimized geometries of  $(\text{H}_2\text{C}_2\text{O}_4)(\text{NH}_3)_n$  ( $n = 1-6$ ) at the PW91PW91/6-311++G(3df,3pd) level of theory (red for oxygen, white for hydrogen, gray for carbon and blue for nitrogen).

an extension of AIM.<sup>80</sup> Not only can the location of the pairwise atoms connected along the bond path be identified, but also the properties around the BCPs can be visualized using NCI. The reduced density gradient is able to be used to confirm non-covalent interactions and covalent interactions in real space.<sup>82</sup> Therefore, the NCI index is a useful tool to distinguish and

visualize different types of non-covalent interactions as regions of real space. The green to blue color coded regions of the bonding isosurface indicate where the hydrogen-bonding interaction is becoming stronger. The reduced gradient isosurfaces ( $s = 0.05$  a.u.) (using the Multiwfn program<sup>67</sup> and VMD program<sup>68</sup>) of Fig. 2 agree with the AIM analysis. In the regions between the

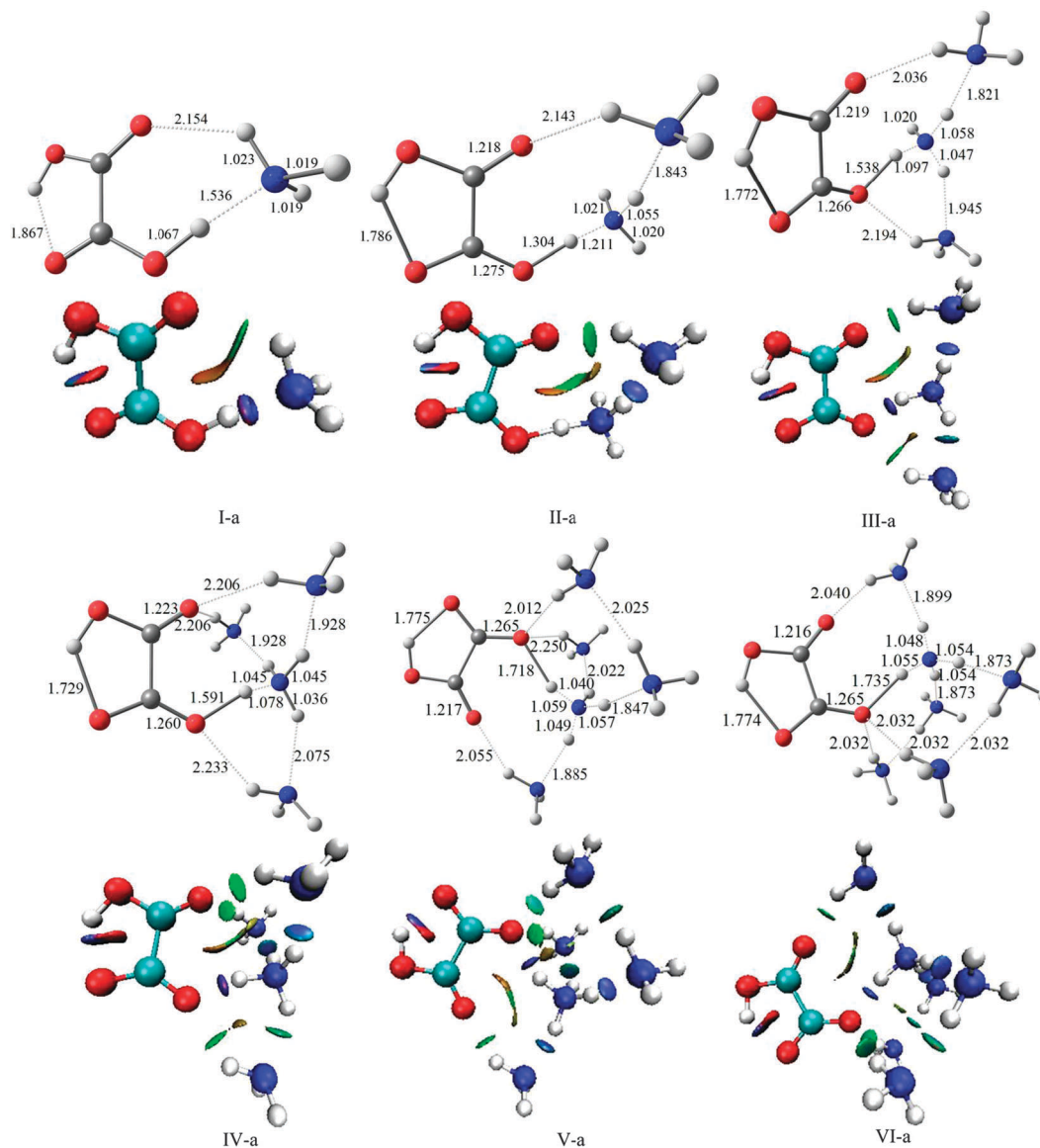


Fig. 2 The lowest-energy structures of the  $(\text{H}_2\text{C}_2\text{O}_4)(\text{NH}_3)_n$  ( $n = 1-6$ ) clusters at the PW91PW91/6-311++G(3df,3pd) level of theory, ordered by the state of association (I, II, III, IV, V, VI). The intramolecular and intermolecular interaction distances and the corresponding isosurfaces are given.

intermolecular nitrogen and hydrogen atoms, the intermolecular oxygen and hydrogen atoms, as well as the intramolecular oxygen and hydrogen atoms, there exist bonding isosurfaces. Here, it is observed that both stronger and weaker intermolecular hydrogen bonds exist in the oxalic acid and ammonia system. Some intermolecular hydrogen bonds are relatively stronger. In Fig. 2, the phenomenon of proton transfer can also be seen. Proton transfer occurs in the tetramer, which is consistent with the AIM results.

### 3.3 Temperature dependence of conformational populations

As is known from the previous studies,<sup>58</sup> as the systems grow larger and form more complexes, the stability order of the isomers may change. Temperature effects could also contribute to the variation of the relative populations of the isomers. Thus the temperature dependence of the thermodynamic properties is an important parameter to understand the roles of the specific nucleation

mechanisms at various atmospheric temperatures. Experiments at lower temperature ranges are difficult to perform due to the increased wall losses of the clusters  $(\text{H}_2\text{C}_2\text{O}_4$  and  $\text{NH}_3$ ) at low temperatures. Here quantum chemical calculations can provide such data. In this work, the temperature dependence of energy for the formation of  $\text{H}_2\text{C}_2\text{O}_4$  and  $\text{NH}_3$  complexes was calculated at temperatures of 100, 150, 200, 250, 298.15, 300, 350 and 400 K.

Considering the Boltzmann distribution of the lower energy isomers, here we used the Boltzmann averaged Gibbs free energy to study the flatness of the potential energy surfaces of  $(\text{H}_2\text{C}_2\text{O}_4)(\text{NH}_3)_n$  ( $n = 1-6$ ). The equations are as follows:

$$\eta_n^i = \frac{e^{-\frac{-\Delta\Delta G_n^i}{k_B T}}}{\sum_i e^{-\frac{-\Delta\Delta G_n^i}{k_B T}}} \quad (3)$$

**Table 4** Topological parameters at intermolecular bond critical points (BCPs) between oxalic acid and ammonia of all global minima at the PW91PW91/6-311++G(3df,3pd) level. The subscripts are used to mark the carbon atoms of different carbonyls

Isomer	BCP	$\rho$	$\nabla^2\rho$	$E$	$G$	$V$	$-G/V$
I-a	HOOC <sub>1</sub> C <sub>2</sub> OO-H...NH <sub>3</sub>	0.0853	0.0136	-0.0400	0.0434	-0.0835	0.52
	NH <sub>2</sub> -H...OHOC <sub>1</sub> C <sub>2</sub> OOH	0.0178	0.0668	0.0024	0.0143	-0.0118	1.21
II-a	HOOC <sub>1</sub> C <sub>2</sub> OO...H-NH <sub>3</sub> NH <sub>3</sub>	0.1359	-0.0796	-0.0967	0.0768	-0.1735	0.44
	NH <sub>3</sub> NH <sub>2</sub> -H...OHOC <sub>1</sub> C <sub>2</sub> OOH	0.0106	0.0394	0.0012	0.0086	-0.0074	1.16
III-a	HOOC <sub>1</sub> C <sub>2</sub> OO...H-NH <sub>3</sub> (NH <sub>3</sub> ) <sub>2</sub>	0.0742	0.1013	-0.0263	0.0516	-0.0779	0.66
	(NH <sub>3</sub> ) <sub>2</sub> NH <sub>2</sub> -H...OHOC <sub>1</sub> C <sub>2</sub> OOH	0.0192	0.0769	0.0028	0.0164	-0.0135	1.21
	(NH <sub>3</sub> ) <sub>2</sub> NH <sub>2</sub> -H...OHOC <sub>1</sub> C <sub>2</sub> OOH	0.0146	0.0538	0.0021	0.0113	-0.0092	1.23
IV-a	HOOC <sub>1</sub> C <sub>2</sub> OO...H-NH <sub>3</sub> (NH <sub>3</sub> ) <sub>3</sub>	0.0645	0.1069	-0.0197	0.0464	-0.0661	0.70
	(NH <sub>3</sub> ) <sub>3</sub> NH <sub>2</sub> -H...OHOC <sub>1</sub> C <sub>2</sub> OOH	0.0136	0.0503	0.0020	0.0105	-0.0085	1.24
	(NH <sub>3</sub> ) <sub>3</sub> NH <sub>2</sub> -H...OHOC <sub>1</sub> C <sub>2</sub> OOH	0.0136	0.0503	0.0020	0.0105	-0.0085	1.24
	(NH <sub>3</sub> ) <sub>3</sub> NH <sub>2</sub> -H...OHOC <sub>1</sub> C <sub>2</sub> OOH	0.0129	0.0488	0.0021	0.0101	-0.0081	1.25
V-a	HOOC <sub>1</sub> C <sub>2</sub> OO...H-NH <sub>3</sub> (NH <sub>3</sub> ) <sub>4</sub>	0.0473	0.1087	-0.0082	0.0354	-0.0436	0.81
	(NH <sub>3</sub> ) <sub>4</sub> NH <sub>2</sub> -H...OHOC <sub>1</sub> C <sub>2</sub> OOH	0.0225	0.0748	0.0015	0.0172	-0.0158	1.09
	(NH <sub>3</sub> ) <sub>4</sub> NH <sub>2</sub> -H...OHOC <sub>1</sub> C <sub>2</sub> OOH	0.0180	0.0741	0.0029	0.0156	-0.0127	1.23
	(NH <sub>3</sub> ) <sub>4</sub> NH <sub>2</sub> -H...OHOC <sub>1</sub> C <sub>2</sub> OOH	0.0131	0.0461	0.0017	0.0098	-0.0081	1.21
VI-a	HOOC <sub>1</sub> C <sub>2</sub> OO...H-NH <sub>3</sub> (NH <sub>3</sub> ) <sub>5</sub>	0.0446	0.1054	-0.0072	0.0335	-0.0407	0.82
	(NH <sub>3</sub> ) <sub>5</sub> NH <sub>2</sub> -H...OHOC <sub>1</sub> C <sub>2</sub> OOH	0.0215	0.0717	0.0015	0.0164	-0.0149	1.10
	(NH <sub>3</sub> ) <sub>5</sub> NH <sub>2</sub> -H...OHOC <sub>1</sub> C <sub>2</sub> OOH	0.0215	0.0717	0.0015	0.0164	-0.0149	1.10
	(NH <sub>3</sub> ) <sub>5</sub> NH <sub>2</sub> -H...OHOC <sub>1</sub> C <sub>2</sub> OOH	0.0186	0.0764	0.0029	0.0161	-0.0132	1.22

$$\Delta G_n = \sum_i n_i^i \Delta G_n^i \quad (4)$$

where

$$\Delta G_n^i = G_n^i - G^{C_2O_4H_2} - nG^{NH_3} \quad (5)$$

$$\Delta \Delta G_n^i = \Delta G_n^i - \min\{\Delta G_n^i\} \quad (6)$$

Here  $i$  and  $n$  represent the isomer order in a cluster and the number of NH<sub>3</sub> respectively. The temperature dependence of the conformational populations for  $n = 4$ ,  $n = 5$  and  $n = 6$  is shown in Fig. 3–5, respectively. It is obvious that the global minimum has the greatest weight in the ensemble of energetically accessible conformers in the range of 100 K to 400 K. As the temperature increases, the weight of the global minimum decreases, and the roles of other local minima become competitive.

For  $n = 4$  (Fig. 3), the global minimum IV-a carries the highest weight, but its weight has a declining trend from 100 K to 400 K. The conformation population of the isomer IV-b increases with increasing temperature, but is still below that of the global minimum at 400 K; further investigation is required to determine whether this isomer competes with the global minimum at temperatures above 400 K. The conformational population of the isomer IV-c increases with increasing temperature up to 300 K and then decreases as the temperature further increases to 400 K. The isomers of IV-e, IV-f, IV-g and IV-h have similar trends to IV-d. In addition, the electronic energy effect can be seen from the competing role of these isomers.

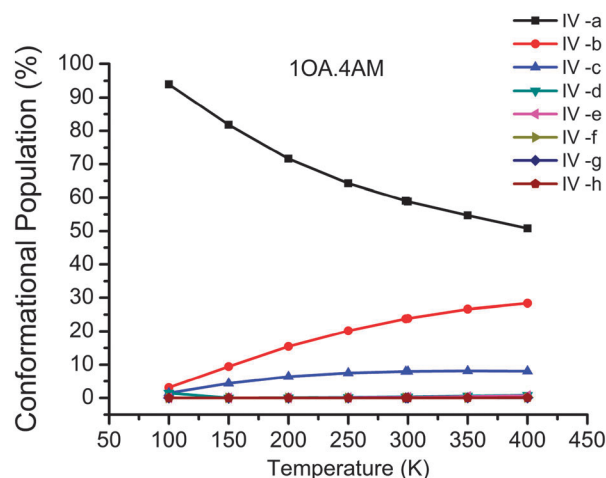


**Fig. 3** The conformational population changes in the low-energy isomers of (H<sub>2</sub>C<sub>2</sub>O<sub>4</sub>)(NH<sub>3</sub>)<sub>4</sub> as a function of temperature (OA stands for oxalic acid, AM stands for ammonia).

For  $n = 5$  (Fig. 4), the global minimum V-a has greater weight than other low-lying isomers below temperatures of approximately 400 K. Below 200 K, the conformational populations of both V-c and V-d have less weight than V-b; however, the trend is reversed when the temperature exceeds 200 K. In addition, the electronic energy effect can be observed from the competing roles of V-c and V-d because their electronic energies are quite close to that of the global minimum (energy differences of 1.04 kcal mol<sup>-1</sup> and 1.232 kcal mol<sup>-1</sup>, respectively).

For  $n = 6$  (Fig. 5), the competitive local minimum (VI-b) has a higher weight than other local minima when the temperature is above 150 K, and its proportion increases with the

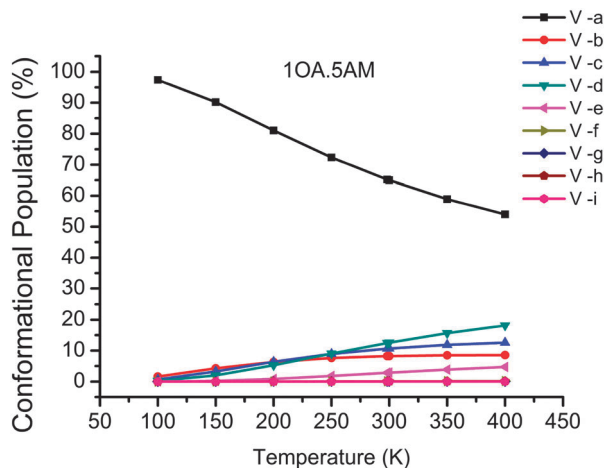


Fig. 4 The conformational population changes in the low-energy isomers of  $(\text{H}_2\text{C}_2\text{O}_4)(\text{NH}_3)_5$  as a function of temperature (OA stands for oxalic acid, AM stands for ammonia).

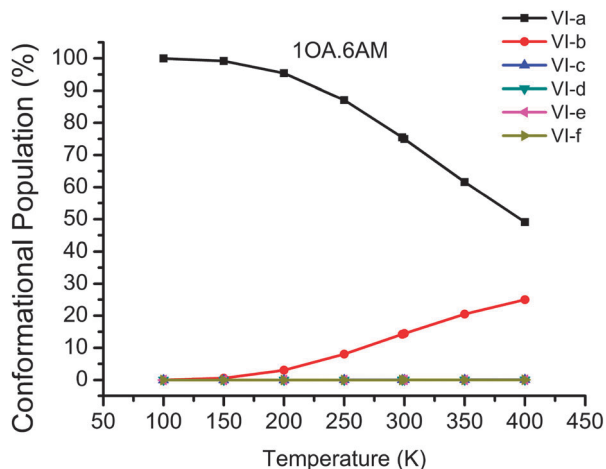


Fig. 5 The conformational population changes in the low-energy isomers of  $(\text{H}_2\text{C}_2\text{O}_4)(\text{NH}_3)_6$  as a function of temperature (OA stands for oxalic acid, AM stands for ammonia).

increasing temperature. The other isomers, VI-c, VI-d, VI-e and VI-f have the same trend from 100 K to 400 K.

The Gibbs free energy of  $(\text{H}_2\text{C}_2\text{O}_4)(\text{NH}_3)_n$  ( $n = 4-6$ ) at different temperatures proves that the coupling of the contributions of various isomers and temperature effects could change the relative stabilities of  $(\text{H}_2\text{C}_2\text{O}_4)(\text{NH}_3)_n$  ( $n = 4-6$ ). The present study focuses on  $(\text{H}_2\text{C}_2\text{O}_4)(\text{NH}_3)_n$  clusters, so no  $\text{H}_2\text{O}$  molecules were included in the complex models. Although  $\text{H}_2\text{O}$  molecules are not included in the calculations, the present work still provides important information for the understanding of cluster formation processes of  $\text{NH}_3$  and  $\text{H}_2\text{C}_2\text{O}_4$  molecules. Investigation of  $\text{H}_2\text{O}$  effects are part of our future research.

### 3.4 Thermodynamics of cluster formation

Thermodynamic analyses can provide insight into the realizability and possibility of cluster formation. Gibbs free energy

changes are used for evaluating the strength of the intermolecular interaction and the spontaneity of the process of the clusters formation. As shown in Table 3, the calculated thermodynamic parameters (ZPE-corrected binding energies at 0 K, enthalpies and Gibbs free energy changes at 298.15 K) for  $n = 1-6$  clusters were acquired by thermal corrections using the PW91PW91 correction and single point electronic energies from DF-MP2-F12 theory as described in the methods section. In Table 3 we see that the formation of the heterodimer of oxalic acid and ammonia is exothermic by  $14.094 \text{ kcal mol}^{-1}$ , and the formation of the trimer of one oxalic acid with two ammonia molecules is exothermic by  $20.539 \text{ kcal mol}^{-1}$ . The formation of a cluster containing one oxalic acid and three ammonia molecules is exothermic by  $28-34 \text{ kcal mol}^{-1}$ , and  $32-37 \text{ kcal mol}^{-1}$  is released during the formation of the  $(\text{H}_2\text{C}_2\text{O}_4)(\text{NH}_3)_4$  cluster. For the formation of the  $(\text{H}_2\text{C}_2\text{O}_4)(\text{NH}_3)_5$  and  $(\text{H}_2\text{C}_2\text{O}_4)(\text{NH}_3)_6$  clusters,  $40-44 \text{ kcal mol}^{-1}$  and  $45-51 \text{ kcal mol}^{-1}$  are released, respectively. The calculation results of Gibbs free energies at room temperature are as follows:  $-5.147 \text{ kcal mol}^{-1}$  for the dimerization of one oxalic acid with one ammonia molecule,  $-2.404 \text{ kcal mol}^{-1}$  to  $-0.797 \text{ kcal mol}^{-1}$  for the trimerization of one oxalic acid with two ammonia molecules,  $1.558$  to  $-6.018 \text{ kcal mol}^{-1}$  for the  $(\text{H}_2\text{C}_2\text{O}_4)(\text{NH}_3)_3$  cluster,  $-1.449$  to  $3.405 \text{ kcal mol}^{-1}$  for the  $(\text{H}_2\text{C}_2\text{O}_4)(\text{NH}_3)_4$  cluster,  $0.522$  to  $5.744 \text{ kcal mol}^{-1}$  for the  $(\text{H}_2\text{C}_2\text{O}_4)(\text{NH}_3)_5$  cluster, and  $3.495$  to  $9.129 \text{ kcal mol}^{-1}$  for the  $(\text{H}_2\text{C}_2\text{O}_4)(\text{NH}_3)_6$  cluster. The Boltzmann averaged Gibbs energies for the formation of  $(\text{H}_2\text{C}_2\text{O}_4)(\text{NH}_3)_n$  clusters are displayed in Table 3. At room temperature, the Gibbs free energies of the clusters range from  $-6.297 \text{ kcal mol}^{-1}$  for dimerization to  $9.129 \text{ kcal mol}^{-1}$  for the formation of the  $(\text{H}_2\text{C}_2\text{O}_4)(\text{NH}_3)_n$  ( $n = 1-6$ ) cluster. Clearly, thermodynamics favors the association of oxalic acid with up to four ammonia molecules at room temperature.

Additionally, as shown in Fig. 6, the  $\Delta G$  values of the global minima of the  $(\text{H}_2\text{C}_2\text{O}_4)(\text{NH}_3)_n$  ( $n = 1-6$ ) clusters increase throughout the temperature range from 100 K to 400 K, which may predict that the stability of the global minima becomes lower with increasing temperature. On the other hand, these clusters may be the favored forms in low temperature conditions.

### 3.5 Atmospheric relevance

Determining the concentrations of the various oxalic acid with ammonia clusters under a given realistic atmospheric condition is of interest. The concentrations can provide a possible reference for the existence in the atmosphere of the corresponding clusters. Briefly, the equilibrium constants  $K_n$  for the formation of the clusters from the respective monomers were calculated from the standard free energies ( $\Delta G_{298.15\text{K}}$ ) using the relation given in eqn (7):

$$\Delta G = -RT \ln(K_n) \quad (7)$$

For the reaction given in eqn (8), the corresponding equilibrium constant  $K_n$  is defined by relation given in eqn (9):

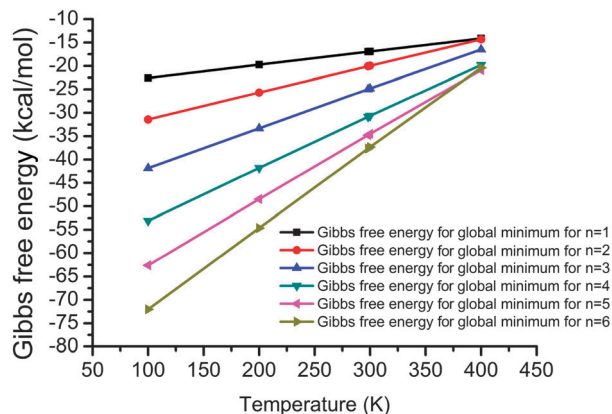
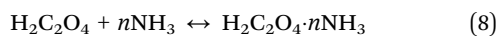


Fig. 6 The Gibbs free energy changes (in kcal mol<sup>-1</sup>) for the global minima of the (H<sub>2</sub>C<sub>2</sub>O<sub>4</sub>)(NH<sub>3</sub>)<sub>n</sub> (*n* = 1–6) clusters depending on temperature at the PW91PW91/6-311++G(3df,3pd) level of theory.



$$K_n = \frac{[\text{C}_2\text{O}_4\text{H}_2 \cdot n\text{NH}_3]}{[\text{NH}_3]^n [\text{C}_2\text{O}_4\text{H}_2]} \quad (9)$$

A quantity referred to as the relative population fraction (RPF) is then defined by the relation given in eqn (10):

$$\text{RPF} = \frac{[\text{C}_2\text{O}_4\text{H}_2 \cdot n\text{NH}_3]}{[\text{C}_2\text{O}_4\text{H}_2]} = K_n [\text{NH}_3]^n \quad (10)$$

The total concentrations of ammonia and oxalic acid were chosen to be 1 and 5 ppb, respectively;<sup>45,46</sup> both of these values correspond to typical and reasonable concentrations of these pollutant species. These calculations were performed for all clusters, and the results are listed in Table 5. The H<sub>2</sub>C<sub>2</sub>O<sub>4</sub>–NH<sub>3</sub> clusters are predicted to have a concentration of 8.02 × 10<sup>5</sup> molecules per cm<sup>3</sup> in the atmosphere. Clearly, the real situation in the atmosphere is much more complicated, and these calculations represent a simplistic and limited approximation. However, these results provide a general estimation of the importance of various clusters. Table 5 also shows the relative population fractions (RPF) calculated at 298.15 K for (H<sub>2</sub>C<sub>2</sub>O<sub>4</sub>)(NH<sub>3</sub>)<sub>n</sub> (*n* = 1–4). From the results of (H<sub>2</sub>C<sub>2</sub>O<sub>4</sub>)(NH<sub>3</sub>)<sub>3</sub> and (H<sub>2</sub>C<sub>2</sub>O<sub>4</sub>)(NH<sub>3</sub>)<sub>4</sub>, it seems that the lower energy forms of the clusters are usually more effective binders of ammonia, and their relatively higher populations give them greater contributions to the atmospheric population. However, the concentrations of the clusters gradually decrease with the binding of more ammonia molecules. They are found in concentrations 10<sup>6</sup>–10<sup>12</sup> fold more dilute. Especially for *n* = 4, the clusters show infinitesimal populations at typical boundary layer atmospheric temperatures, which could be due to the relatively lower concentration of ammonia than oxalic acid in the atmosphere.

### 3.6 Optical properties

Aerosols weaken light by scattering and absorbing, and the extinction properties have a great impact on atmospheric visibility and radiative forcing.<sup>83,84</sup> The light scattering properties of particles, clusters and molecules in the atmosphere are

Table 5 Gibbs free energy<sup>a</sup> values in kcal mol<sup>-1</sup>, relative bound percentages<sup>b</sup> (RPF × 100%) and estimated concentrations for the stable clusters of (H<sub>2</sub>C<sub>2</sub>O<sub>4</sub>)(NH<sub>3</sub>)<sub>n</sub> (*n* = 1–4). The estimated atmospheric concentrations are based on an oxalic acid concentration of 5 ppb and an ammonia concentration of 1 ppb

<i>n</i>	Isomers	Δ <i>G</i> (kcal mol <sup>-1</sup> )	RPF × 100%	Molecules per cm <sup>3</sup>
1	I-a	-5.149	5.96 × 10 <sup>-4</sup>	8.02 × 10 <sup>5</sup>
2	II-a	-2.404	5.79 × 10 <sup>-15</sup>	7.79 × 10 <sup>-6</sup>
	II-b	0.821	2.50 × 10 <sup>-17</sup>	3.36 × 10 <sup>-8</sup>
3	III-a	-6.018	2.59 × 10 <sup>-21</sup>	3.49 × 10 <sup>-12</sup>
	III-b	-5.689	1.49 × 10 <sup>-21</sup>	2.00 × 10 <sup>-12</sup>
	III-c	-6.297	4.16 × 10 <sup>-21</sup>	5.59 × 10 <sup>-12</sup>
	III-d	-5.671	1.44 × 10 <sup>-21</sup>	1.94 × 10 <sup>-12</sup>
	III-e	-1.405	1.07 × 10 <sup>-24</sup>	1.44 × 10 <sup>-15</sup>
	III-f	-1.558	1.39 × 10 <sup>-24</sup>	1.87 × 10 <sup>-15</sup>
4	IV-a	-1.449	1.16 × 10 <sup>-33</sup>	1.55 × 10 <sup>-24</sup>
	IV-b	-0.911	4.66 × 10 <sup>-34</sup>	6.27 × 10 <sup>-25</sup>
	IV-c	-0.264	1.56 × 10 <sup>-34</sup>	2.10 × 10 <sup>-25</sup>

<sup>a</sup> PW91PW91/6-311++G(3df,3pd) results. <sup>b</sup> With respect to the corresponding clusters.

related to the wavelength of the incoming light and their size. When the diameters are much lower than the wavelength of the incoming radiation, Rayleigh scattering is the dominant mechanism.<sup>70,85,86</sup> Jonas Elm and his co-workers found that the Rayleigh scattering intensity depends quadratically on the number of water molecules in clusters, and that even a single ammonia molecule is able to induce a high anisotropy, which further increases the scattering intensity.<sup>70</sup> Additionally, Rayleigh scattering is also used to analyse hydrogen-bonded systems with *ab initio* calculations.<sup>87–90</sup>

The depolarization ratios and Rayleigh scattering intensities for the perpendicular and parallel components of linear polarized light for the (H<sub>2</sub>C<sub>2</sub>O<sub>4</sub>)(NH<sub>3</sub>)<sub>n</sub> systems were calculated at the CAM-B3LYP/aug-cc-pVDZ level of theory. The isotropic mean polarizabilities  $\bar{\alpha}$  are quite size dependent and vary linearly with a correlation coefficient of  $\rho = 0.99986$ , as shown in Fig. 7(c), consistent with the study of methanol clusters and chloride hydration clusters.<sup>58,90</sup> In Fig. 7, the Rayleigh light scattering intensity of natural light,  $\mathfrak{R}_n$ , and the depolarization ratios,  $\rho_n$ , of the (H<sub>2</sub>C<sub>2</sub>O<sub>4</sub>)(NH<sub>3</sub>)<sub>n</sub> clusters can be seen as a function of the number of ammonia molecules in the cluster. The non-linear dependence of  $\mathfrak{R}_n$  on the number of ammonia molecules is observed to closely follow the trend of a second order polynomial, consistent with the results of sulfuric acid hydration systems and chloride hydration systems.<sup>58,70</sup> This increasing trend can be attributed to the gradually increasing binding polarizability of the clusters, such that the  $(\bar{\alpha})^2$  term in eqn (6) will dominate in the Rayleigh scattering of larger particles. The calculated depolarization ratios  $\rho_n$  are observed to become smaller as the cluster grows. This is due to the increase in the mean isotropic polarizability with the number of molecules, in combination with the anisotropic polarizability being relatively constant in the range of 27–35 a.u. This is consistent with what is to be expected as the clusters change from molecular clusters into spherical isotropic particles. Additionally, the depolarization ratios for clusters with 1–6 ammonia molecules are seen to fluctuate from 0.006 to 0.05.

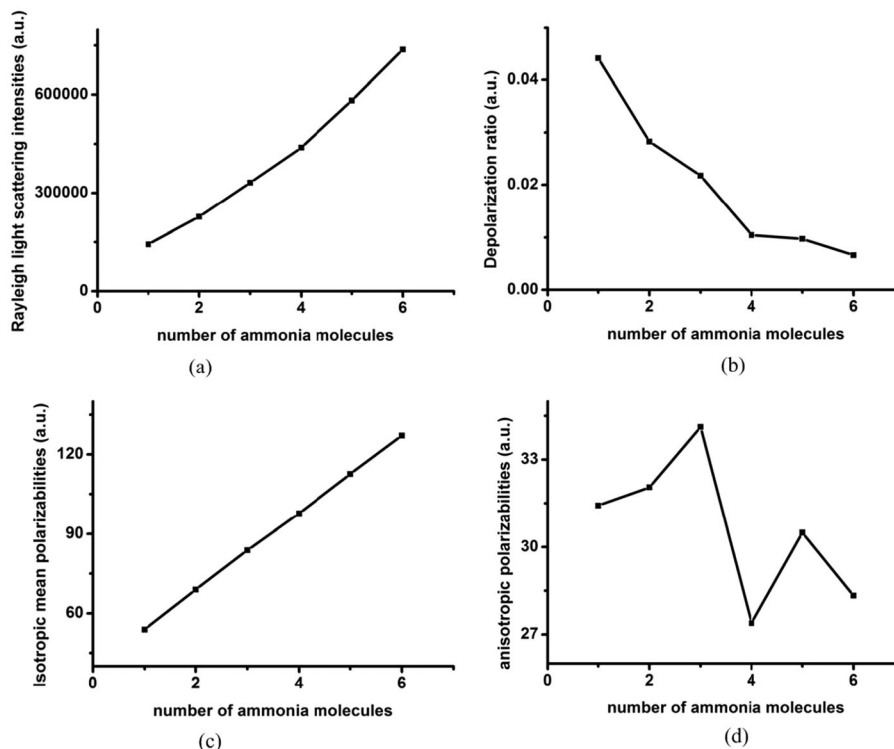


Fig. 7 The Rayleigh light scattering and cluster polarizability properties: (a) Rayleigh light scattering intensities as a function of the number of ammonia molecules; (b) depolarization ratio as a function of the number of ammonia molecules; (c) isotropic mean polarizabilities as a function of the number of ammonia molecules; (d) anisotropic polarizabilities as a function of the number of ammonia molecules.

From the earlier research investigating the relevance of the number of hydrogen bonds on cluster polarizability,<sup>58,91</sup> we have fitted the calculated isotropic mean polarizability values as a linear function of cluster size  $n$ ,  $\bar{n}_{\text{O-H}}$  and  $\bar{n}_{\text{N-H}}$ :

$$\bar{\alpha} = a + b \times n + c \times \bar{n}_{\text{O-H}} + d \times \bar{n}_{\text{N-H}}$$

where  $n_{\text{O-H}} = \frac{n_{\text{O-H}}}{n}$  and  $\bar{n}_{\text{N-H}} = \frac{n_{\text{N-H}}}{n}$  represent the average number of O–H hydrogen bonds and number of N–H hydrogen bonds, respectively. The fit is found to be excellent with a correlation coefficient of 0.99993. This indicates that the O–H hydrogen bonds and N–H hydrogen bonds both contribute to the cluster polarizability.

## Conclusion

In the present study, we investigated the interaction of common organic oxalic acid with ammonia and their hydrogen bonded complexes using DFT calculations. The structure of  $(\text{H}_2\text{C}_2\text{O}_4)(\text{NH}_3)_n$  agreed well with earlier reports; ionization events and cluster growth were also studied. The present study led to these findings:

(a)  $(\text{H}_2\text{C}_2\text{O}_4)(\text{NH}_3)_n$  ( $n = 1-6$ ) clusters exhibit very strong hydrogen bonds; in other words, oxalic acid interacts strongly with ammonia. The analyses of bond length, interaction energy and electron density indicated that three ammonia molecules are needed to ionize oxalic acid, forming an  $\text{HC}_2\text{O}_4^-/\text{NH}_4^+$  ion pair.

(b) The thermodynamics and concentration results indicate that oxalic acid probably forms clusters with ammonia in the atmosphere. The Gibbs free energy of the global minima at different temperatures indicates that oxalic and ammonia clusters may form more favorably under low temperature conditions. Analyzing the contributions of the various isomers to the conformational populations, the configurations with the lowest energies are observed with higher concentration than other isomers of the same size. Thus the small populations of the configurations with lower energy can almost be ignored. The  $(\text{H}_2\text{C}_2\text{O}_4)(\text{NH}_3)_n$  clusters with an obvious concentration are predicted to be present in the atmosphere, and they could likely participate in the process of new particle formation. However, the concentrations of clusters gradually decreases with the binding of more ammonia molecules. Especially for  $n = 4$ , the clusters show infinitesimal populations at typical boundary layer atmospheric temperatures, which could be due to the relatively lower concentration of ammonia than oxalic acid in the atmosphere.

(c) Our study serves as the first scattering investigation of relevance to  $(\text{H}_2\text{C}_2\text{O}_4)(\text{NH}_3)_n$  ( $n = 1-6$ ) clusters. We found that the Rayleigh scattering intensities and the isotropic mean polarizabilities depend on the number of ammonia molecules. Additionally, the hydrogen bonds are also found to contribute to the cluster polarizability. The impact of ammonia and ammonium molecules on the subsequent nucleation of oxalic acid in Rayleigh scattering activities needs to be further studied.

The current work is fundamental and necessary for our further study of prenucleation clusters containing a mixture of oxalic acid, ammonia, ammonium, water and sulfuric acid. This work predicts the possible forms of oxalic acid with ammonia when participating in nucleation in a theoretical approach, and more theoretical and experimental studies are still needed to elucidate the nucleation mechanism.

## Acknowledgements

The study was supported by grants from the National Natural Science Foundation of China (Grant No. 21403244 and 21133008), the National High Technology Research and Development Program of China (863 Program) (Grant No. 2014AA06A501), and the “Interdisciplinary and Cooperative Team” of CAS. Acknowledgement is also given to the “Thousand Youth Talents Plan”. The computation was performed in EMSL, a national scientific user facility sponsored by the Department of Energy’s Office of Biological and Environmental Research and located at Pacific Northwest National Laboratory (PNNL). PNNL is a multi-program national laboratory operated for the DOE by Battelle. Part of the computation was performed at the Supercomputing Center of the Chinese Academy of Sciences and Supercomputing Center of USTC.

## References

- R. J. Charlson, S. Schwartz, J. Hales, R. D. Cess, J. J. Coakley, J. Hansen and D. Hofmann, *Science*, 1992, **255**, 423–430.
- M. Kulmala, H. Vehkamäki, T. Petäjä, M. Dal Maso, A. Lauri, V.-M. Kerminen, W. Birmili and P. H. McMurry, *J. Aerosol Sci.*, 2004, **35**, 143–176.
- G. Oberdörster and M. Utell, *Environ. Health Perspect.*, 2002, **110**, A440.
- D. B. Kittelson, W. Watts and J. Johnson, *Atmos. Environ.*, 2004, **38**, 9–19.
- A. Saxon and D. Diaz-Sanchez, *Nat. Immunol.*, 2005, **6**, 223–226.
- W. Xu and R. Zhang, *J. Phys. Chem. A*, 2012, **116**, 4539–4550.
- B. R. Bzdek and M. V. Johnston, *Anal. Chem.*, 2010, **82**, 7871–7878.
- T. Kurtén, T. Petäjä, J. Smith, I. Ortega, M. Sipilä, H. Junninen, M. Ehn, H. Vehkamäki, L. Mauldin and D. Worsnop, *Atmos. Chem. Phys.*, 2011, **11**, 3007–3019.
- J. Almeida, S. Schobesberger, A. Kürten, I. K. Ortega, O. Kupiainen-Määttä, A. P. Praplan, A. Adamov, A. Amorim, F. Bianchi and M. Breitenlechner, *Nature*, 2013, **502**, 359–363.
- H. Keskinen, A. Virtanen, J. Joutsensaari, G. Tsagkogeorgas, J. Duplissy, S. Schobesberger, M. Gysel, F. Riccobono, J. G. Slowik and F. Bianchi, *Atmos. Chem. Phys.*, 2013, **13**, 5587–5600.
- T. Jokinen, M. Sipilä, H. Junninen, M. Ehn, G. Lönn, J. Hakala, T. Petäjä, R. Mauldin III, M. Kulmala and D. Worsnop, *Atmos. Chem. Phys.*, 2012, **12**, 4117–4125.
- K. D. Froyd and E. R. Lovejoy, *J. Phys. Chem. A*, 2011, **116**, 5886–5899.
- T. I. Yacovitch, N. Heine, C. Brieger, T. Wende, C. Hock, D. M. Neumark and K. R. Asmis, *J. Phys. Chem. A*, 2013, **117**, 7081–7090.
- H. R. Leverentz, J. I. Siepmann, D. G. Truhlar, V. Loukonen and H. Vehkamäki, *J. Phys. Chem. A*, 2013, **117**, 3819–3825.
- O. Kupiainen, I. Ortega, T. Kurtén and H. Vehkamäki, *Atmos. Chem. Phys.*, 2012, **12**, 3591–3599.
- J. Elm, M. Fard, M. Bilde and K. V. Mikkelsen, *J. Phys. Chem. A*, 2013, **117**, 12990–12997.
- P. Paasonen, T. Olenius, O. Kupiainen, T. Kurtén, T. Petäjä, W. Birmili, A. Hamed, M. Hu and L. Huey, *Atmos. Chem. Phys.*, 2012, **12**, 9113–9133.
- J. Wang and A. S. Wexler, *Geophys. Res. Lett.*, 2013, **40**, 2834–2838.
- J. Elm, M. Bilde and K. V. Mikkelsen, *J. Chem. Theory Comput.*, 2012, **8**, 2071–2077.
- J. Elm, M. Bilde and K. V. Mikkelsen, *Phys. Chem. Chem. Phys.*, 2013, **15**, 16442–16445.
- M. Rozenberg, A. Loewenschuss and C. J. Nielsen, *J. Phys. Chem. A*, 2014, **118**, 1004–1011.
- R. Zhang, *Science*, 2010, **328**, 1366–1367.
- L. Wang, A. F. Khalizov, J. Zheng, W. Xu, Y. Ma, V. Lal and R. Zhang, *Nat. Geosci.*, 2010, **3**, 238–242.
- R. Zhang, A. Khalizov, L. Wang, M. Hu and W. Xu, *Chem. Rev.*, 2011, **112**, 1957–2011.
- D. Yue, M. Hu, R. Zhang, Z. Wang, J. Zheng, Z. Wu, A. Wiedensohler, L. He, X. Huang and T. Zhu, *Atmos. Chem. Phys.*, 2010, **10**, 4953–4960.
- B. Temelso, T. N. Phan and G. C. Shields, *J. Phys. Chem. A*, 2012, **116**, 9745–9758.
- A. J. Prenni, P. J. DeMott, S. M. Kreidenweis, D. E. Sherman, L. M. Russell and Y. Ming, *J. Phys. Chem. A*, 2001, **105**, 11240–11248.
- B. Zobrist, C. Marcolli, T. Koop, B. Luo, D. Murphy, U. Lohmann, A. Zardini, U. Krieger, T. Corti and D. Cziczo, *Atmos. Chem. Phys.*, 2006, **6**, 3115–3129.
- B. Kärcher and T. Koop, *Atmos. Chem. Phys.*, 2005, **5**, 703–714.
- R. Wagner, O. Möhler, H. Saathoff, M. Schnaiter and T. Leisner, *Atmos. Chem. Phys.*, 2011, **11**, 2083–2110.
- H. Giebl, A. Berner, G. Reischl, H. Puxbaum, A. Kasper-Giebl and R. Hitznerberger, *J. Aerosol Sci.*, 2002, **33**, 1623–1634.
- F. Yu and R. P. Turco, *Geophys. Res. Lett.*, 2000, **27**, 883–886.
- A. B. Nadykto and F. Yu, *Phys. Rev. Lett.*, 2004, **93**, 016101.
- Y. Xu, A. B. Nadykto, F. Yu, J. Herb and W. Wang, *J. Phys. Chem. A*, 2009, **114**, 387–396.
- R. Zhang, L. Wang, A. F. Khalizov, J. Zhao, J. Zheng, R. L. McGraw and L. T. Molina, *Proc. Natl. Acad. Sci. U. S. A.*, 2009, **106**, 17650–17654.
- A. B. Nadykto and F. Yu, *Chem. Phys. Lett.*, 2007, **435**, 14–18.
- Y. Yokouchi and Y. Ambe, *Atmos. Environ. (1967-1989)*, 1986, **20**, 1727–1734.
- K. Kawamura and K. Ikushima, *Environ. Sci. Technol.*, 1993, **27**, 2227–2235.

- 39 H. A. Khwaja, *Atmos. Environ.*, 1995, **29**, 127–139.
- 40 K. Kawamura, H. Kasukabe and L. A. Barrie, *Atmos. Environ.*, 1996, **30**, 1709–1722.
- 41 X.-F. Huang, M. Hu, L.-Y. He and X.-Y. Tang, *Atmos. Environ.*, 2005, **39**, 2819–2827.
- 42 P. K. Martinelango, P. K. Dasgupta and R. S. Al-Horr, *Atmos. Environ.*, 2007, **41**, 4258–4269.
- 43 P. Liu, W. Leaitch, C. Banic, S. M. Li, D. Ngo and W. Megaw, *J. Geophys. Res.*, 1996, **101**, 28971–28990.
- 44 Y. Xu, A. B. Nadykto, F. Yu, L. Jiang and W. Wang, *THEOCHEM*, 2010, **951**, 28–33.
- 45 K. H. Weber, F. J. Morales and F.-M. Tao, *J. Phys. Chem. A*, 2012, **116**, 11601–11617.
- 46 K. H. Weber, Q. Liu and F.-M. Tao, *J. Phys. Chem. A*, 2014, **118**, 1451–1468.
- 47 J.-W. Yoon, J.-H. Park, C.-C. Shur and S.-B. Jung, *Microelectron. Eng.*, 2007, **84**, 2552–2557.
- 48 D. J. Wales and J. P. Doye, *J. Phys. Chem. A*, 1997, **101**, 5111–5116.
- 49 W. Huang, R. Pal, L.-M. Wang, X. C. Zeng and L.-S. Wang, *J. Chem. Phys.*, 2010, **132**, 054305.
- 50 L.-M. Wang, R. Pal, W. Huang, X. C. Zeng and L.-S. Wang, *J. Chem. Phys.*, 2010, **132**, 114306.
- 51 W. Huang, H.-J. Zhai and L.-S. Wang, *J. Am. Chem. Soc.*, 2010, **132**, 4344–4351.
- 52 W. Huang and L.-S. Wang, *Phys. Rev. Lett.*, 2009, **102**, 153401.
- 53 W. Huang, M. Ji, C.-D. Dong, X. Gu, L.-M. Wang, X. G. Gong and L.-S. Wang, *ACS Nano*, 2008, **2**, 897–904.
- 54 W. Huang, A. P. Sergeeva, H.-J. Zhai, B. B. Averkiev, L.-S. Wang and A. I. Boldyrev, *Nat. Chem.*, 2010, **2**, 202–206.
- 55 L.-L. Yan, Y.-R. Liu, T. Huang, S. Jiang, H. Wen, Y.-B. Gai, W.-J. Zhang and W. Huang, *J. Chem. Phys.*, 2013, **139**, 244312.
- 56 Y.-R. Liu, H. Wen, T. Huang, X.-X. Lin, Y.-B. Gai, C.-J. Hu, W.-J. Zhang and W. Huang, *J. Phys. Chem. A*, 2014, **118**, 508–516.
- 57 S. Jiang, Y. R. Liu, T. Huang, H. Wen, K. M. Xu, W. X. Zhao, W. J. Zhang and W. Huang, *J. Comput. Chem.*, 2014, **35**, 159–165.
- 58 S. Jiang, T. Huang, Y.-R. Liu, K.-M. Xu, Y. Zhang, Y.-Z. Lv and W. Huang, *Phys. Chem. Chem. Phys.*, 2014, **16**, 19241–19249.
- 59 B. Delley, *J. Phys. Chem. A*, 1990, **92**, 508–517.
- 60 H. Wen, Y. R. Liu, K. M. Xu, T. Huang, C. J. Hu, W. J. Zhang and W. Huang, *Chin. J. Chem. Phys.*, 2013, **26**, 729–738.
- 61 K.-M. Xu, T. Huang, H. Wen, Y.-R. Liu, Y.-B. Gai, W.-J. Zhang and W. Huang, *RSC Adv.*, 2013, **3**, 24492–24502.
- 62 Y.-P. Zhu, Y.-R. Liu, T. Huang, S. Jiang, K.-M. Xu, H. Wen, W.-J. Zhang and W. Huang, *J. Phys. Chem. A*, 2014, **118**, 7959–7974.
- 63 M. Frisch, G. Trucks, H. B. Schlegel, G. Scuseria, M. Robb, J. Cheeseman, G. Scalmani, V. Barone, B. Mennucci and G. Petersson, *Gaussian 09, Revision A. 02*, Gaussian, Inc., Wallingford, CT, 2009, vol. 200.
- 64 H. J. Werner, P. J. Knowles, G. Knizia, F. R. Manby and M. Schütz, *Wiley Interdiscip. Rev.: Comput. Mol. Sci.*, 2012, **2**, 242–253.
- 65 H. Werner, P. Knowles, G. Knizia, F. Manby, M. Schütz, P. Celani, T. Korona, R. Lindh, A. Mitrushenkov and G. Rauhut, MOLPRO, version 2010.1, a package of ab initio programs.
- 66 R. F. W. Bader, *Atoms in Molecules: A Quantum Theory*, Oxford University Press, Oxford, UK, 1990.
- 67 T. Lu, *Multwfn: A Multifunctional Wavefunction Analyzer, Version 3.0.1*, 2013, <http://multwfn.codeplex.com>.
- 68 W. Humphrey, A. Dalke and K. Schulten, VMD: visual molecular dynamics, *J. Mol. Graphics*, 1996, **14**, 33–38, <http://www.ks.uiuc.edu/Research/vmd/>.
- 69 E. R. Johnson, S. Keinan, P. Mori-Sanchez, J. Contreras-Garcia, A. J. Cohen and W. Yang, *J. Am. Chem. Soc.*, 2010, **132**, 6498–6506.
- 70 J. Elm, P. Norman, M. Bilde and K. V. Mikkelsen, *Phys. Chem. Chem. Phys.*, 2014, **16**, 10883–10890.
- 71 J. Kauczor, P. Norman and W. A. Saidi, *J. Chem. Phys.*, 2013, **138**, 114107.
- 72 P. A. Limacher, K. V. Mikkelsen and H. P. Lüthi, *J. Chem. Phys.*, 2009, **130**, 194114.
- 73 P. Lind, M. Carlsson, B. Eliasson, E. Glimsdal, M. Lindgren, C. Lopes, L. Boman and P. Norman, *Mol. Phys.*, 2009, **107**, 629–641.
- 74 H. Solheim, K. Ruud, S. Coriani and P. Norman, *J. Chem. Phys.*, 2008, **128**, 094103.
- 75 T. Fahleson, J. Kauczor, P. Norman and S. Coriani, *Mol. Phys.*, 2013, **111**, 1401–1404.
- 76 B. F. Milne, P. Norman, F. Nogueira and C. Cardoso, *Phys. Chem. Chem. Phys.*, 2013, **15**, 14814–14822.
- 77 D. Cremer and E. Kraka, *Angew. Chem., Int. Ed. Engl.*, 1984, **23**, 627–628.
- 78 N. Han, Y. Zeng, X. Li, S. Zheng and L. Meng, *J. Phys. Chem. A*, 2013, **117**, 12959–12968.
- 79 U. Koch and P. Popelier, *J. Phys. Chem.*, 1995, **99**, 9747–9754.
- 80 J. Contreras-García, W. Yang and E. R. Johnson, *J. Phys. Chem. A*, 2011, **115**, 12983–12990.
- 81 A. J. Cohen, P. Mori-Sánchez and W. Yang, *Science*, 2008, **321**, 792–794.
- 82 X. Yang, L. Gan, L. Han, E. Wang and J. Wang, *Angew. Chem.*, 2013, **125**, 2076–2080.
- 83 J. H. Seinfeld and S. N. Pandis, *John Wiley & Sons Inc*, Hoboken, New Jersey, 2012, pp. 691–711.
- 84 Y. Chan, R. Simpson, G. H. McTainsh, P. D. Vowles, D. Cohen and G. Bailey, *Atmos. Environ.*, 1999, **33**, 3237–3250.
- 85 J. Strutt, *Philos. Mag.*, 1871, **41**, 107–120, 274–279.
- 86 J. Strutt, *Philos. Mag.*, 1881, **12**, 81–101.
- 87 E. Rissi, E. E. Fileti and S. Canuto, *Theor. Chem. Acc.*, 2003, **110**, 360–366.
- 88 E. E. Fileti, R. Rivelino and S. Canuto, *J. Phys. B: At., Mol. Opt. Phys.*, 2003, **36**, 399.
- 89 P. Chaudhuri and S. Canuto, *THEOCHEM*, 2006, **760**, 15–20.
- 90 E. Orestes, P. Chaudhuri and S. Canuto, *Mol. Phys.*, 2012, **110**, 297–306.
- 91 T. K. Ghanty and S. K. Ghosh, *J. Chem. Phys.*, 2003, **118**, 8547–8550.